

Atomistic modelling of the channeling process with radiation reaction force included

Gennady B. Sushko, Andrei V. Korol and Andrey V. Solov'yov

MBN Research Center, Altenhöferallee 3, 60438 Frankfurt am Main, Germany

Abstract. Methodology is developed that incorporates the radiative reaction force into the relativistic molecular dynamics framework implemented in the MBN EXPLORER software package. The force leads to a gradual decrease in the projectile's energy ε due to the radiation emission. This effect is especially strong for ultra-relativistic projectiles passing through oriented crystals where they experience the action of strong electrostatic fields as has been shown in recent experiments. A case study has been carried out for the initial approbation of the methodology developed. Simulations of the processes of planar channeling and photon emission have been performed for 150 GeV positrons in a 200 μm thick single oriented Si(110) crystal. Several regimes for the decrease in ε have been established and characterized. Further steps in developing the code to include the necessary quantum corrections are identified and possible algorithmic modifications are proposed.

1. Introduction

In the last decade, a number of experiments have been carried out at different accelerator facilities studying various phenomena related to the interaction of ultra-relativistic beams of multi-GeV charged projectiles with oriented crystals of different types and geometries [1–16]. In these experiments the basic effect of channeling has been exploited for the beam manipulation (beam steering, focusing, collimation, splitting, and extraction) as well as for the generation of intensive electromagnetic radiation.

The channeling phenomenon stays for a specific motion of a charged projectile in an oriented crystal along a crystallographic plane (planar channeling) or an axis (axial channeling) due to correlated interactions with the lattice atoms. A comprehensive theoretical study by Lindhard [17] has demonstrated that the penetration through a crystal strongly depends on the orientation of the particle's velocity with respect to crystallographic directions. The continuum potential model [17] explains the channeling motion in terms of the action of a collective electrostatic field of the atomic planes.‡ The field, being repulsive for positively charged particles, steers them into the interplanar region so that they move along the planar direction between two neighboring planes experiencing, simultaneously, so-called channeling oscillations in the transverse direction. Negatively charged particles, being attracted by the field, channel in the

‡ To be specific, we refer to the planar channeling.

vicinity of a plane. Channeling motion may occur in linear crystals as well as in bent [18] and periodically bent [19] crystals.

Channeling oscillations give rise to a specific type of electromagnetic radiation, - the channeling radiation (ChR) [20]. A strongly correlated motion of the channeling particle in the collective crystalline field results in a much higher intensity of ChR as compared to the intensity of the incoherent bremsstrahlung radiation emitted by the same projectile in the amorphous medium, see e.g. [21].

A charged particle moving in a medium (more generally, in an external field) loses its energy due to the emission of electromagnetic radiation. For ultra-relativistic electrons and positrons of very high energies (tens of GeV and above) the radiative energy loss greatly exceed the losses due to the ionizing collisions [22]. Therefore, the radiation damping, i.e. the process of a gradual decrease in the particle's energy due to radiation, must be accounted for an accurate quantitative analysis of the projectile motion.

Recent experiments with multi-GeV light projectiles (50 GeV positrons and 40-80 GeV electrons) passing through silicon and diamond oriented crystals at small angles to the crystallographic axial and planar directions have shown the necessity to incorporate the radiative recoil in describing the dynamics of the channeling particles [11, 16]. A theoretical scheme based on the continuous potential concept has been developed [15, 16] and convincing agreement with experiment has been demonstrated.

Various approximations have been used to simulate channeling phenomenon in oriented crystals. Whilst most rigorous description relies on the framework of quantum mechanics (see Ref. [23] and references therein), the classical description in terms of particles trajectories can be applied to high-energy projectiles (hundred MeV range and above) [24, 25]. Simulation of the channeling and related phenomena within the framework of continuum potential model has been implemented in several software packages, see Ref. [26] for a description of the most recent ones. For the purpose of the current paper we mention the code described in [27] and a more recent one presented in [28] (see also [15, 16]). These codes integrate the classical equations of motion of an ultra-relativistic particle traversing oriented crystals with account for (i) the continuous interplanar potential, and (ii) the radiative damping force in the form presented in [29].

Numerical simulations of the channeling and radiation processes beyond the continuous potential framework can be carried out by means of the multi-purpose computer package MBN EXPLORER [30]. MBN EXPLORER is a software package for the advanced multiscale simulations of structure and dynamics of complex molecular Meso-Bio-Nano (MBN) systems. It has many unique features and a wide range of applications in physics, chemistry, biology, materials science, industry and medicine [31]. It is suitable for classical non-relativistic and relativistic molecular dynamics (MD), Euler dynamics, reactive [32] and irradiation-driven [33] MD simulations as well as for stochastic dynamics or Monte Carlo simulations of various randomly moving MBN systems or processes [34, 35]. These algorithms are applicable to a large range of molecular systems of different kind, such as nano- and biological systems, nanostructured materials, composite/hybrid materials, gases, plasmas, liquids, solids,

and their interfaces, with the sizes ranging from atomic to mesoscopic. The MBN EXPLORER package is supplemented with special multitask software toolkit MBN STUDIO [36] used to set up and start MBN Explorer calculations, monitor their progress, examine calculation results, visualize inputs and outputs, and analyze specific characteristics determined by the output of simulations.

By means of a special module [37] of the package it is possible to simulate a passage of various particles (positively and negatively charged, light and heavy) in various media, such as hetero-crystalline structures (including superlattices), straight bent and periodically bent crystals, amorphous solids, liquids, nanotubes, fullerenes, biological environment [37]. The applicability of the code to a particular structure can be adjusted by choosing a proper interaction potential from a large variety of the potentials already included in the package. The software allows one to simulate the classical trajectories within the framework of relativistic MD, i.e. when the speed of a projectile v is comparable to the speed of light, c . Under such condition, in many cases the motion of even light particles (electrons, positrons) can be treated in terms of classical mechanics rather than the quantum mechanics.

Over the last years the module have been extensively applied to simulate the propagation of ultra-relativistic charged particles in oriented crystals accompanied by emission of intensive radiation. A comprehensive description of the multiscale all-atom relativistic molecular dynamics approach implemented in MBN EXPLORER as well as a number of case studies related to modeling channeling and photon emission by ultra-relativistic projectiles (within the sub-GeV up to ten GeV energy range) in straight, bent and periodically bent crystals are presented in a review article [26].

Additional feature that has been implemented in MBN EXPLORER and is discussed in Section 2 below concerns the influence that have the radiation emitted by the particle upon its motion. In terms of classical electrodynamics this influence can be described by introducing a radiative reaction force acting on the projectile, see, e.g. [29, 38]. For ultra-relativistic electrons and positrons of very high energies (tens of GeV and above) this force becomes quite noticeable so that it must be accounted for to properly simulate the motion. Several related case studies are presented in Section 3.

2. Methodology

The 3D simulation procedure of the motion an ultra-relativistic particle in an external field or/and in an atomic environment is based on the formalism of the classical relativistic mechanics and describes the motion in the laboratory reference frame. MBN EXPLORER implements the relativistic equations of motion written in the following form:

$$\begin{cases} \dot{\mathbf{v}} = \frac{1}{m\gamma} (\mathbf{F} - \boldsymbol{\beta} (\mathbf{F} \cdot \boldsymbol{\beta})) \\ \dot{\mathbf{r}} = \mathbf{v} \end{cases}, \quad (1)$$

where $\gamma = \varepsilon/mc^2 = (1 - v^2/c^2)^{-1/2}$ is the relativistic Lorentz factor of a projectile of energy ε and mass m , c is the speed of light, and $\boldsymbol{\beta} = \mathbf{v}/c$.

The force \mathbf{F} acting on the projectile is the sum of two terms:

$$\mathbf{F} = \mathbf{F}_{\text{em}} + \mathbf{F}_{\text{rr}}. \quad (2)$$

The term \mathbf{F}_{em} stands for the total electromagnetic (Lorentz) force due to (i) electrostatic field \mathbf{E} created by atoms of the medium and/or by external sources of electric field, and (ii) external magnetic field \mathbf{B} :

$$\mathbf{F}_{\text{em}} = q(\mathbf{E} + \boldsymbol{\beta} \times \mathbf{B}), \quad (3)$$

where q is the charge of a projectile.

The second term on the right-hand side of Eq. (2) stands for the radiative reaction force, which can be written in the following form [29]:

$$\begin{aligned} \mathbf{F}_{\text{rr}} = & \frac{2q^2}{3mc^3} \left\{ q\gamma \left[\frac{\partial \mathbf{E}}{\partial t} + (\mathbf{v} \cdot \nabla) \mathbf{E} + \boldsymbol{\beta} \times \left(\frac{\partial \mathbf{B}}{\partial t} + (\mathbf{v} \cdot \nabla) \mathbf{B} \right) \right] \right. \\ & \left. + \frac{q}{mc} \left[\mathbf{F} \times \mathbf{B} + q(\boldsymbol{\beta} \cdot \mathbf{E}) \mathbf{E} \right] - \frac{\gamma^2}{mc} \left[\mathbf{F}^2 - q^2(\boldsymbol{\beta} \cdot \mathbf{E})^2 \right] \boldsymbol{\beta} \right\} \end{aligned} \quad (4)$$

where ∇ stands for the vector differential operator with respect to \mathbf{r} .

To accurately integrate highly non-linear equations of motion (1) the fourth-order Runge-Kutta method with adaptive time step control is implemented MBN EXPLORER.

Applied to the propagation in an atomic environment the system (1) describes the classical motion of a particle in an electrostatic field due to the medium atoms. In the absence of a magnetic field and for the stationary electric field only the first term on the right-hand side of Eq. (3) is accounted for while the radiative reaction force reduces to

$$\mathbf{F}_{\text{rr}} = \frac{2q^3}{3mc^3} \left\{ \gamma(\mathbf{v} \cdot \nabla) \mathbf{E} + \frac{q}{mc}(\boldsymbol{\beta} \cdot \mathbf{E}) \mathbf{E} - \frac{q\gamma^2}{mc} \left[\mathbf{E}^2 - (\boldsymbol{\beta} \cdot \mathbf{E})^2 \right] \boldsymbol{\beta} \right\}. \quad (5)$$

Here $\mathbf{E} = \mathbf{E}(\mathbf{r}) = -q^{-1} \nabla U(\mathbf{r})$ with $U(\mathbf{r})$ being the potential energy of the projectile's interaction with the atoms:

$$U(\mathbf{r}) = \sum_j U_{\text{at}}(|\mathbf{r} - \mathbf{r}_j|) \quad (6)$$

where U_{at} are the potentials of individual atoms and \mathbf{r}_j denotes the position vector of the j th atom. The code allows one to evaluate the atomic potential using the approximations due to Molière [39] and Pacios [40]. A rapid decrease of these potentials with increasing the distances from the atoms allows the sum (6) to be truncated in practical calculations. The summation accounts only for the atoms located inside the sphere of a (specified) cut-off radius ρ_{max} with the center at the instant location of the projectile. The value ρ_{max} is chosen large enough to ensure negligible contribution to the sum from the atoms located at $r > \rho_{\text{max}}$. The search for such atoms is facilitated by using the linked cell algorithm implemented in MBN EXPLORER [30, 31]. More details on the algorithms implemented to compute trajectories of the particles passing through a medium on the macroscopic scale are presented in [26, 30].

The system (1) with $\mathbf{F}_{\text{em}} = q\mathbf{E}(\mathbf{r})$ and \mathbf{F}_{rr} from (5) can be applied to any charged projectile moving in a specified atomic environment. To be specific, in what follows

when carrying out quantitative estimates we consider the case of an ultra-relativistic ($\gamma \gg 1$) positron ($q = e$) moving in an oriented silicon crystal.

The applicability of (5) is subject to the condition that the magnitude of the Lorentz force in the co-moving frame (in which the particle is at rest) is small compared to $m^2c^2/e^2 = mc^2/r_0$ ($r_0 \approx 2.818 \times 10^{-13}$ cm is the classical electron radius). This condition leads to the following strong inequality that relates the electric field intensity E and the particle's energy (see Eq. (76.5) in Ref. [29]):

$$eE \ll (eE)_{\max} = \frac{1}{\gamma} \frac{mc^2}{r_0} \approx \frac{10^6}{\varepsilon}. \quad (7)$$

On the right-hand side ε is measured in GeV producing the value of $(eE)_{\max}$ in GeV/cm.

For $\varepsilon = 50$ and 150 GeV positrons Eq. (7) produces $(eE)_{\max} \approx 1.8 \times 10^4$ and 0.6×10^4 GeV/cm, respectively. Describing the positron-atom interaction in terms of the screened Coulomb (Yukawa) potential $Ze \exp(-r/a_{\text{TF}})/r$ with atomic number $Z = 14$ (a silicon atom) and the Thomas-Fermi radius $a_{\text{TF}} = 0.8853Z^{-1/3}a_0 \approx 0.194 \text{ \AA}$, one finds that the values of $(eE)_{\max}$ quoted above are achieved at the distances $r \approx 0.063a_0$ and $0.11a_0$, respectively. In these estimates $a_0 = 0.529 \text{ \AA}$ is the Bohr radius.

General methodology implemented in MBN EXPLORER to generate particles' trajectories in a crystalline environment accounts for randomness in sampling the incoming projectiles (the key factors here are beam size, divergence and direction with respect to the crystal orientation) as well as in displacement of the lattice atoms from the nodal positions due to the thermal vibrations [26,37]. As a result, each trajectory corresponds to a unique crystalline environment and, therefore, all simulated trajectories are statistically independent and can be analyzed further to quantify the channeling process as well as the radiation emitted by projectiles.

The process of radiation emission is sensitive to the magnitude of the quantum strong-field parameter χ defined as follows [22]

$$\chi = \gamma \frac{E}{E_0} = \gamma \frac{eE}{F_0} \quad (8)$$

where $E_0 = 1.32 \times 10^{16}$ V/cm is the critical field and $F_0 = eE_0 = 1.32 \times 10^7$ GeV/cm is the corresponding critical force. Classical description is valid if $\chi < 1$. This implies the restriction on the range of distances between a projectile and an atomic nucleus in individual close-encounter collisions. Using, as above, the Yukawa potential to describe the positron-silicon atom interaction one estimates the distances r_{\min} beyond which the classical framework is applicable:

$$r > r_{\min} \approx \begin{cases} 0.29a_0 & \text{for } \varepsilon = 50 \text{ GeV} \\ 0.41a_0 & \text{for } \varepsilon = 150 \text{ GeV} \end{cases} \quad (9)$$

3. Case study

In this section we present a case study that refers to the $\varepsilon = 150$ GeV positrons channeling in an oriented Si(110) crystal (the interplanar distance $d = 1.92 \text{ \AA}$) of

thickness $L = 200 \mu\text{m}$. The positions of the crystal atoms were generated with account for the atoms' random displacement from the nodes due to thermal vibrations at temperature $T = 300 \text{ K}$. For each atom the displacement was generated by means of the normal distribution with the root-mean-square (rms) amplitude u_T equal to 0.075 \AA [41]. The direction of the incident particles, the z -axis, is chosen along the (110) plane and well away from crystallographic axes of low indices to avoid the axial channeling regime. A projectile enters the crystal at $z = 0$ and exits at $z = L$. The crystal is considered infinitely large in transverse x and y directions. The y -axis is aligned with $\langle 110 \rangle$ axial direction. At the entrance the x and y coordinates of the particle have been randomly generated by means of the uniform distribution within the rectangle $\Delta y = 4d = 7.68 \text{ \AA}$, $\Delta x = 2a = 10.86 \text{ \AA}$ where $a = 5.43 \text{ \AA}$ is the lattice constant. The angular distribution of the positrons at the crystal entrance has been ignored, therefore, the results presented below refer to an ideally collimated beam of zero divergence.

The trajectories have been obtained by integrating classical equations of motion (1). Therefore, it was expected that in the course of molecular dynamics simulation of the particles' propagation through the crystalline medium events of the close-encounter collisions with the crystal atoms would occur in which either condition (7) or condition (9) will not be met. Such events lead to a (noticeable) overestimation of the energy loss due to the radiation emission in a localized spatial region. Hence, important was to evaluate the fraction of the trajectories affected by such collisions.

Figure 1 shows a distribution $\Delta N/N_{\text{tot}}/\text{bin}$ of the particles leaving the crystals as a function of a relative energy loss $\Delta\varepsilon/\varepsilon$. Here $N_{\text{tot}} \approx 10^4$ is the total number of the simulated trajectories, ΔN is the number of trajectories that correspond to a particular interval of the energy loss; the width of each interval (bin) is 0.01. Symbols show the heights of the histogram rectangles (not drawn) and are placed in the bins' centers. Solid vertical lines divide the whole interval $\Delta\varepsilon/\varepsilon = [0, 1]$ into three subintervals and the numbers with per cent sign show the fraction of N_{tot} that falls into each subinterval. Dashed (red) vertical line marks the maximum relative loss equal to 0.045 that can be estimated analytically applying the continuous potential model to describe the positron channeling (see Section Appendix A for the details).

The distribution presented shows that most of the particles, 63 per cent, experience the energy loss $\Delta\varepsilon/\varepsilon \leq 0.1$ that is approximately in accordance with the estimate. However, a noticeable number of the particles, ca 20 %, lose anomalously large fraction of the initial energy ($\Delta\varepsilon/\varepsilon > 0.3$) due to the action of the radiative reaction force. Hence, it is informative to carry out more detailed analysis of the simulated trajectories aiming at revealing the reason for large values of the losses.

Figure 2 presents the distribution of the number ΔN of particles, which channel through the whole crystal, with respect to the average amplitude $\langle a_{\text{ch}} \rangle$ of channeling oscillations calculated along the particles' trajectories. The average amplitude is measured in units of the interplanar distance d so that $\langle a_{\text{ch}} \rangle_{\text{max}}/d = 0.5$. Each graph corresponds to the indicated interval of $\Delta\varepsilon/\varepsilon$. Positron channeling occurs between two neighbouring atomic planes. Hence, the larger channeling amplitude is the closer a

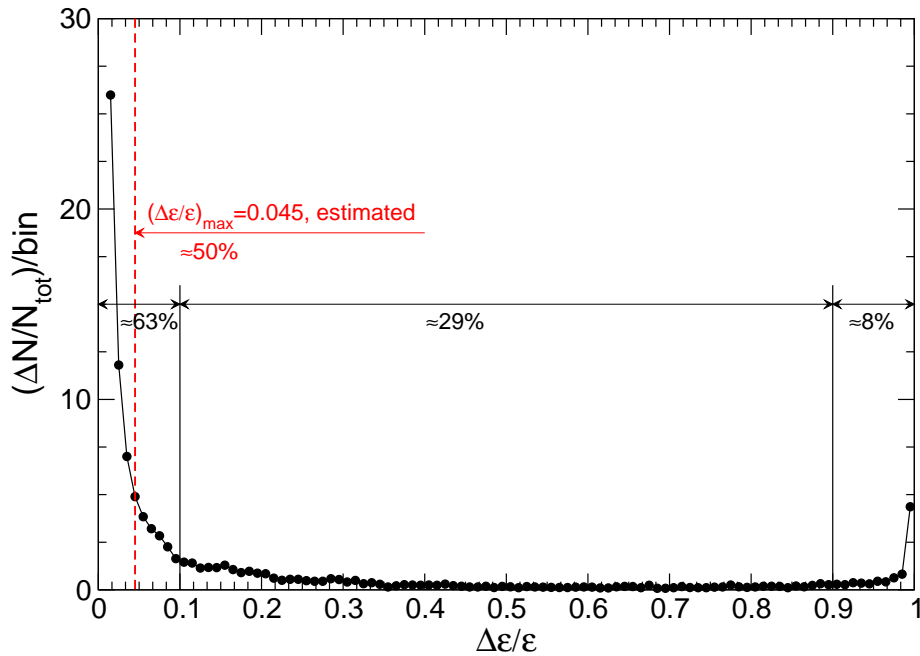


Figure 1. Distribution (a histogram) of positrons at the crystal exit with respect to the relative energy loss, $\Delta\varepsilon/\varepsilon$. Symbols indicate the heights of the histogram rectangles placed in the center of the bins (the bin width is 0.01). Solid vertical lines mark three intervals of $\Delta\varepsilon/\varepsilon$. The values indicated in per cent correspond to the fractions of the total number of trajectories, N_{tot} , moving along which a particle experiences the energy loss within each interval. The vertical dashed line marks the maximum energy loss $(\Delta\varepsilon/\varepsilon)_{\text{max}}$ estimated within the continuous potential framework. Approximately 50 per cent of all trajectories fall in the interval $[0, 0.045]$.

projectile approaches the planes experiencing the action of stronger field in this spatial domain. However, significant energy losses happen not due to the action of the average electrostatic field of a plane but rather during rare individual collisions of the projectile with the atoms that are displaced from the nodal positions due to the thermal vibrations. In more detail this issue is addressed below in the paper, see discussion in connection with Figs. 4 and 5 below.

The dechanneling length L_d of a 150 GeV positron in Si(110), estimated using Eq. (1.50) from Ref. [42], is equal to 8.2 cm, i.e. two orders of magnitude larger than the crystal thickness L used in the simulations. Therefore, most of the particles accepted into the channeling mode at the entrance channel through the whole crystal and their channeling amplitude does not change noticeable in the course of propagation through the crystal. Therefore, for a particle of an ideally collimated beam, the average amplitude is equal, approximately, to the absolute value of the transverse coordinate y_0 measured at the entrance with respect to the geometrical center of the channel, $\langle a_{\text{ch}} \rangle \approx |y_0|$. Figure 3 presents the distribution of the channeling particles with respect to the transverse coordinate y_0 (measured in units of the interplanar distance). Comparing the graphs that refer to the same value of $\Delta\varepsilon/\varepsilon$ in Figs. 2 and 3 one notices a strong correlation between the distributions. To be noted, in particular, are relatively small

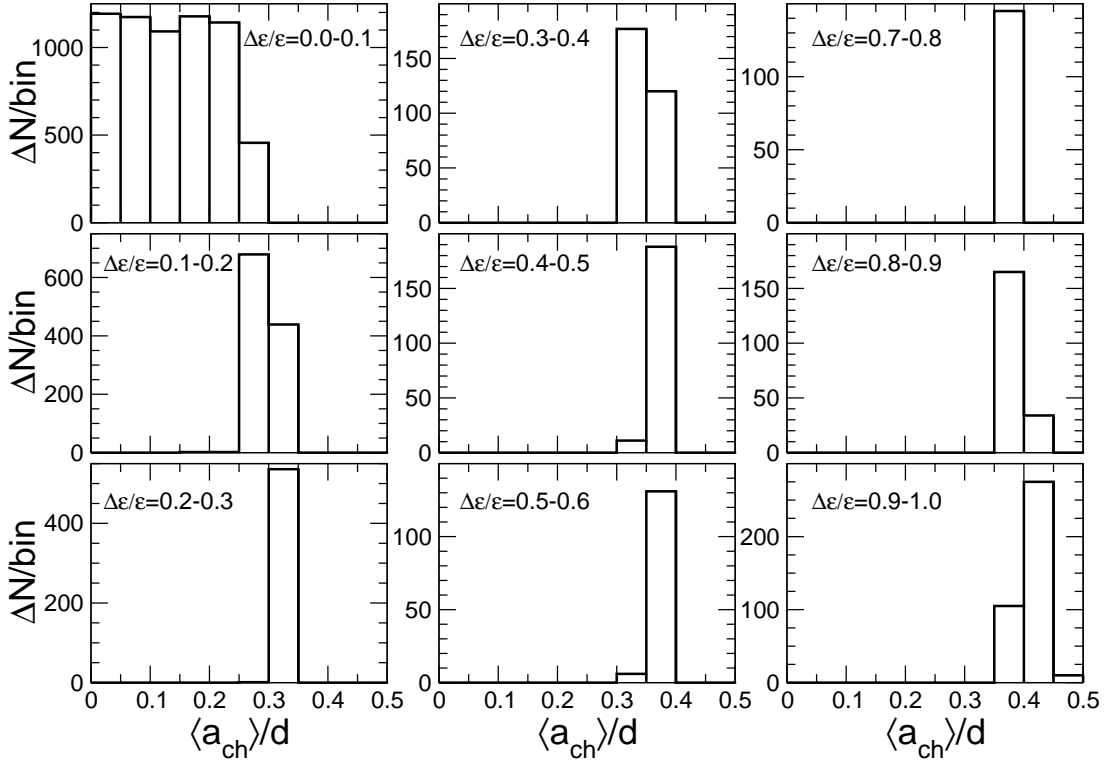


Figure 2. Distribution of projectiles with respect to the average amplitude of channeling oscillations, $\langle a_{\text{ch}} \rangle$, along the trajectory. Nine graphs correspond to different intervals of $\Delta\epsilon/\epsilon$ as indicated in each graph.

numbers of particles that enter the crystal with $|y_0|/d \geq 0.45$ or/and move in the channeling mode with $\langle a_{\text{ch}} \rangle_{\text{max}}/d \geq 0.45$, see the right-bottom graphs in both figures. This range of the coordinates / amplitudes corresponds to the distances from the crystallographic plane approximately equal to the rms amplitude $u_T = 0.075 \text{ \AA}$. In this domain the volume density of the crystal atoms is enhanced due to thermal vibrations so that there is high probability for a projectile to experience a hard collision with the nuclei and, as a result, to leave the channeling mode.

Within the framework of molecular dynamics, the simulation of a projectile's motion is based on solving the equations of motion (1) accounting, as in reality, for the interaction of the projectile with individual atoms of the crystal. The potential energy of this interaction varies rapidly in the course of the projectile's motion in the vicinity of the atomic chains and so does the radiative reaction force \mathbf{F}_{rr} (5). Analysis of each simulated trajectory allows one to establish the spatial regions where the action of \mathbf{F}_{rr} results in significant energy losses.

The top graph in Fig. 4 presents several simulated trajectories (in their projections on the (yz) plane) that correspond to different values of the relative energy loss starting with $\Delta\epsilon/\epsilon = 0.1$ for the uppermost trajectory up to $\Delta\epsilon/\epsilon = 0.9$ (the lowest trajectory) with the increment 0.1. For the sake of convenience the trajectories are shown in separate channels, the geometric borders of which are drawn with dotted lines. The feature to

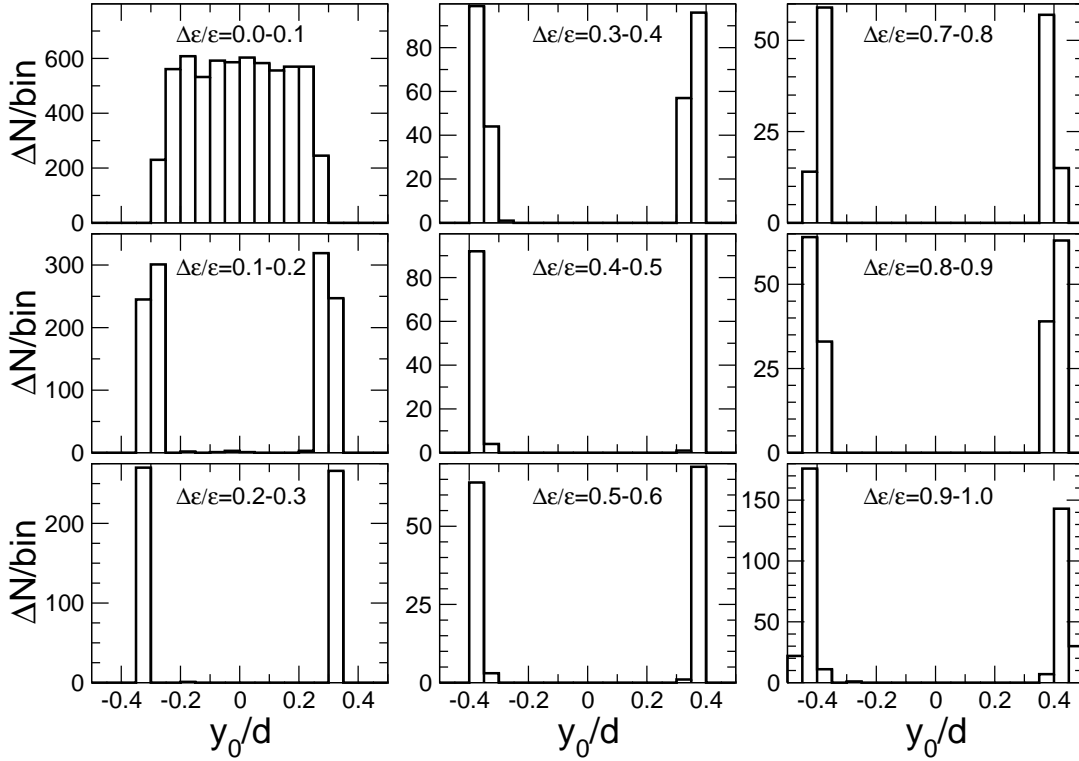


Figure 3. Distribution of projectiles with respect to the coordinate y_0 at the crystal entrance. Nine graphs correspond to different intervals of $\Delta\varepsilon/\varepsilon$ as indicated in each graph. The distributions presented correlate with those shown in Fig. 2.

be noted is the decrease in the period λ_{ch} of channeling oscillations with penetration distance z . The dependence $\lambda_{\text{ch}} \propto \sqrt{\varepsilon(z)}$ is most clearly seen when comparing the periods in the initial and final segments of the trajectories with $\Delta\varepsilon/\varepsilon \geq 0.5$ and relates the segments to the corresponding parts of dependencies $\varepsilon = \varepsilon(z)$ that are shown in the bottom graph. The value of $\Delta\varepsilon/\varepsilon$ is indicated for each dependence. Vertical grid lines, drawn in each graph, help one to correlate the $\varepsilon = \varepsilon(z)$ dependencies with the trajectories.

Two upper trajectories that correspond to $\Delta\varepsilon/\varepsilon = 0.1$ and 0.2 refer to the channeling oscillations with the average amplitudes $\langle a_{\text{ch}} \rangle/d = 0.25$ and 0.32 , respectively. Hence, they stay away from the atomic planes and experience, on average, the action of a relatively uniform interplanar field which results, in turn, in a smooth gradual decrease of the energy with the penetration distance.

Larger values of the relative energy loss correspond to the motion with larger amplitudes, see Fig. 2. Projectiles that move along such trajectories spend more time in close vicinity to the atomic plane and thus have higher probability to successively collide with several atoms. In each collision the particle experiences a localized action of much stronger atomic field. As a result, the dependence $\varepsilon = \varepsilon(z)$, being still a monotonously decreasing one, becomes modulated: the segments of a relatively weak decrease, which corresponds to the motion well away from the planes, alternate with

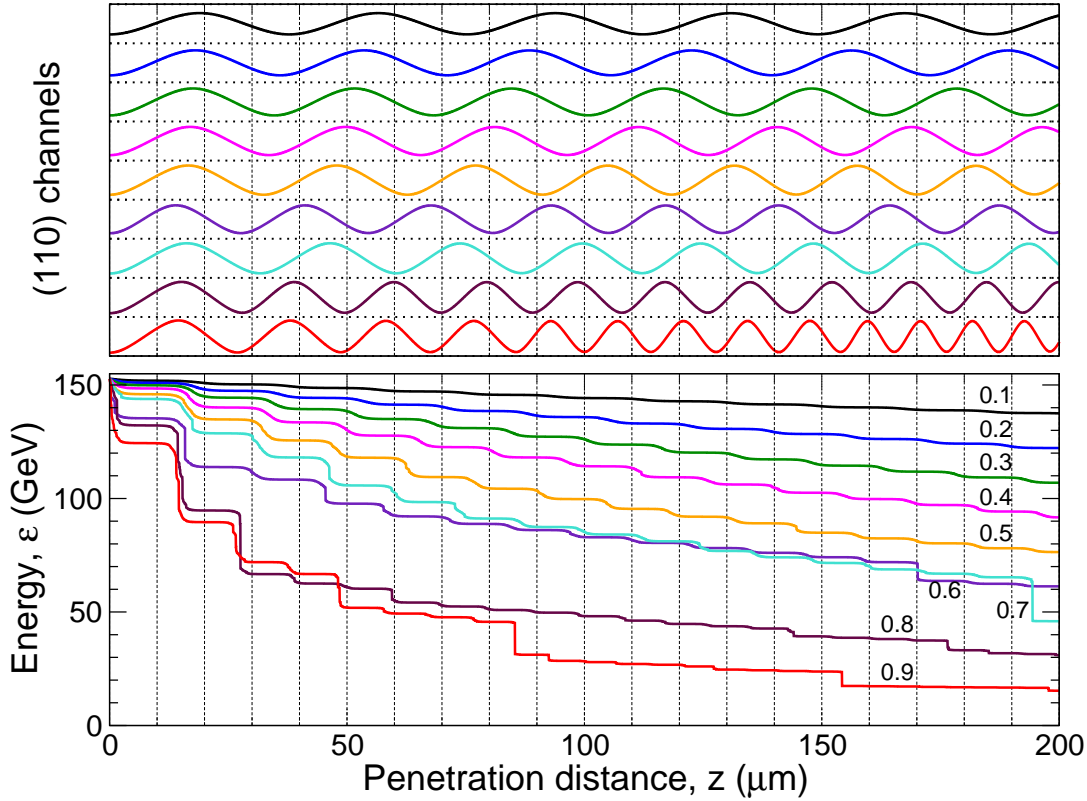


Figure 4. *Top:* Selected simulated trajectories (in projection on the (yz) -plane) of 150 GeV positrons in an oriented silicon(110) crystal. The z -axis is directed along the incoming projectiles, the (xz) -plane is parallel to the crystallographic planes (dotted horizontal lines), and the y -axis is perpendicular to the planes. The trajectories correspond to different values of the relative energy loss: Starting with $\Delta\varepsilon/\varepsilon = 0.1$ for the top trajectory up to $\Delta\varepsilon/\varepsilon = 0.9$ for the lowest trajectory with the increment 0.1. *Bottom:* Dependencies $\varepsilon = \varepsilon(z)$ of the projectile energy on the penetration distance z calculated for the trajectories shown on the top graph. The value of $\Delta\varepsilon/\varepsilon$ is indicated for each dependence.

the segments of a steeper decrease due to the collisions with atoms. The modulations of this type are well pronounced in the $\varepsilon = \varepsilon(z)$ dependencies shown in Fig. 4 *bottom* for $\Delta\varepsilon/\varepsilon = 0.3, 0.4,$ and 0.5 . The period of modulation equals to the half-period of the channeling oscillations, see the corresponding trajectories in the top graph. The length of the segments of the steeper decrease is of the order of several microns, which means that the projectile experiences a number of sequential collisions.

Significant energy loss can occur in a close collision of a projectile with a constituent atom. Such events reveal themselves as sharp step-like change of the function $\varepsilon = \varepsilon(z)$, see the curves for $\Delta\varepsilon/\varepsilon \geq 0.6$ in Fig. 4 *bottom*. In more detail this feature is illustrated by Fig. 5, which shows the segment of the simulated trajectory (top), dependence $\varepsilon(z)$ (middle) and the transverse component of the total electrostatic force acting on the projectile (bottom) over a short path, $\Delta z = 6 \text{ \AA}$. In the course of simulations the equations of motion (1) were integrated with the time step $\delta t = 10^{-4}$ femtoseconds,

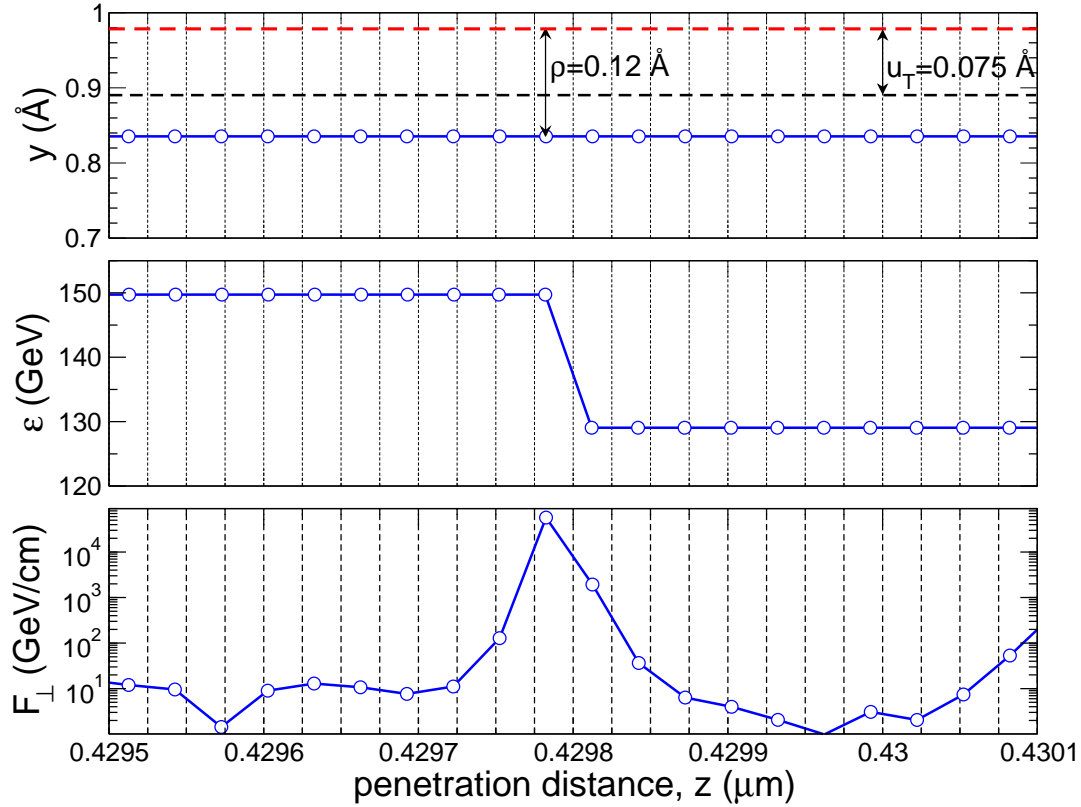


Figure 5. *Top:* Solid line with open circles shows a short segment of the simulated trajectory of a 150 GeV positron in the vicinity, $\rho = 0.12 \text{ \AA}$, of a geometric border (thick dashed line) of the Si(110) planar channel. Thin solid line marks the distance from the border equal to the rms thermal vibration amplitude u_T . The transverse coordinate y is measured from the channel geometric center.

Middle: The projectile's energy versus the penetration distance, $\varepsilon = \varepsilon(z)$.

Bottom: The transverse component of the electrostatic force acting on the particle.

which was also set as the output step. The open circles in the figure represent the output data that are separated by $\delta z \approx c\delta t \approx 0.3 \text{ \AA}$.

The dependence $\varepsilon = \varepsilon(z)$ exhibits a sharp decrease, $\Delta\varepsilon/\varepsilon \approx 0.2$, at $z \approx 0.42978 \mu\text{m}$ due to a single close collision with a crystal atom. In such a collision the impact parameter b is smaller than the atomic screening radius, therefore, the collision effectively occurs in the point Coulomb field of the nucleus. Using Eqs. (B.1) and (B.2) one estimates (within the classical framework) the impact parameter that corresponds to the quoted value of the relative energy loss: $b \approx 0.09a_{\text{TF}} \approx 1.7 \times 10^{-2} \text{ \AA}$.[§] Moving along the trajectory shown in Fig. 4 *top* the projectile passes at the distance $\rho = 0.12 \text{ \AA}$ from the geometric border of the channel. This value is order of magnitude larger than the impact parameter, therefore, to make the collision happen the atom must be displaced from its nodal position by distances within the interval

[§] The scattering angle in such collision, calculated using Eq. (B.3), $\theta_s \approx 0.16 \mu\text{rad}$ is small compared to the Lindhard critical angle $\theta_L = \sqrt{2U_0/\varepsilon} \approx 17 \mu\text{rad}$, where $U_0 \approx 22 \text{ eV}$ is the depth of the continuous potential well in Si(110), see Table A1.

$[\rho - b, \rho + b]$. The probability $\Delta P(\rho, b)$ of such displacement one estimates by means of the Gaussian distribution: $\Delta P(\rho, b) \approx (2b/\sqrt{2\pi u_T^2}) \exp(-\rho^2/2u_T^2) \approx 5 \times 10^{-2}$. This estimate shows, that the probability of a large energy loss in a single collision is high enough for projectiles experience channeling oscillations with sufficiently large amplitude, $a_{\text{ch}} \gtrsim d/2 - ku_T$ with $k = 1 \dots 3$. A particle that channels with large amplitude over a macroscopic distance can experience several events of close collisions, see the dependencies corresponding to $\Delta\varepsilon/\varepsilon \geq 0.6$ in Fig. 4.

Figure 5 *bottom* shows the variation of the transverse component F_{\perp} of the electrostatic force. As the particle approaches the atom the force increases sharply reaching the value $F_{\perp} \approx 7 \times 10^4$ GeV/cm in the point of the collision. Such a force does not satisfy the condition (7) and also it results in a large value $\chi \gg 1$ of the quantum strong-field parameter, Eq. (8). Therefore, in the vicinity of the points of close collisions the classical approach to the particle dynamics and the radiation emission is not applicable. Instead, the description within the framework of quantum electrodynamics must be used. However, important is that the quantum collisional and radiation processes are random, fast and localized in space. Therefore, they can be incorporated into the framework of classical molecular dynamics in a stochastic manner with the probabilities elaborated on the basis of quantum mechanics / electrodynamics. This can be achieved because the aforementioned quantum processes happen on the sub-femtosecond time scales (i.e., during the periods comparable or smaller than a typical single time step of the simulations). Such methodology has been already implemented in the MBN EXPLORER software package for atomistic simulations of the irradiation-driven transformations of complex molecular systems [33].

Most of the simulated trajectories are free from the aforementioned difficulties and can be used for the statistical analysis of other processes, for example, the radiation emission. Figure 6 presents spectral distribution $\dot{E}/(\hbar\omega)$ of the channeling radiation emitted by 150 GeV positrons within the cone $\theta = 6/\gamma \approx 20 \mu\text{rad}$ along the direction of incident particles. The calculations have been performed for the trajectories simulated with (solid curve without symbols) and without (solid curves with symbols) account for the radiative reaction force F_{rr} . In the former case only those trajectories were taken into account that satisfied the condition $\Delta\varepsilon/\varepsilon \leq 0.1$. Top left graph in Fig. 2 indicates that the condition is fulfilled for all trajectories for which average amplitude of the channeling oscillations does not exceed $d/4$ as well as a large fraction of the trajectories for which $0.25 < \langle a_{\text{ch}} \rangle / d \leq 0.3$. Overall number of such trajectories is nearly two thirds of the total number of simulated trajectories, see Fig. 1. The resulting spectral dependence was calculated as the average of the spectra emitted from each trajectory. The details of the numerical procedures can be found in Refs. [26, 37].

To assess the extent to which the radiative reaction force affects the radiation emission one has to simulate trajectories assuming $F_{\text{rr}} = 0$ and calculate the resulting spectral distribution. However, prior to calculating the distribution a certain procedure must be applied to select the trajectories that can be matched to those accounted for when calculating $\dot{E}/(\hbar\omega)$ with $F_{\text{rr}} \neq 0$. The criterion for the selection relies on matching

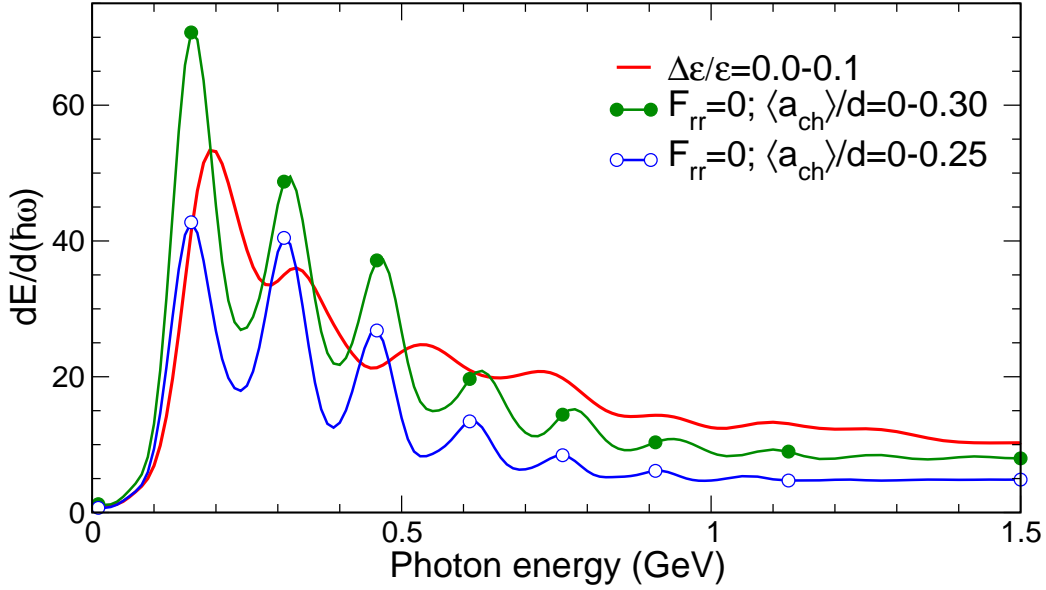


Figure 6. Spectral distribution of channeling radiation emitted by 150 GeV positrons in 200 μm thick Si(110) crystal. Solid (red) curve without symbols presents the dependence calculated for the trajectories that correspond to the interval $\Delta\varepsilon/\varepsilon = 0 - 0.1$ of the relative energy losses due to the radiative reaction force F_{rr} . Solid curves with symbols show the spectra calculated for the trajectories without account for F_{rr} and selected with respect to the ranges for the average amplitude of channeling oscillations, $\langle a_{\text{ch}} \rangle$, as indicated in the legend. See also explanations in the text.

the average amplitude of the channeling oscillations. Two curves with symbols in Fig. 6 show the spectral distributions calculated by averaging the distributions of radiation emitted from the trajectories for which the value of $\langle a_{\text{ch}} \rangle/d$ falls into the ranges indicated in the caption. All three curves exhibit the undulator-type spectral dependence: the presence of equidistant peaks that correspond to the emission into several first harmonics of the channeling radiation. In the absence of the radiative reaction force the channeling oscillations of the positrons are nearly harmonic, so that their frequency Ω_{ch} does not depend on the amplitude a_{ch} and stays constant in the course of motion. This results in a series of well-pronounced and well separated peaks the positions of which ω_n ($n = 1, 2, 3, \dots$) are related to Ω_{ch} through $\omega_n = 2\gamma^2 n \Omega_{\text{ch}} / (1 + K^2/2)$, where $K \approx 2\pi\gamma a_{\text{ch}}/\lambda_{\text{ch}}$ is the so-called undulator parameter, λ_{ch} stands for the spatial period of the oscillations. The radiative reaction force, acting mainly in the longitudinal direction, decelerates the particle leading to the increase in the channeling oscillations frequency along the trajectory, $\Omega_{\text{ch}}(z) \propto (\varepsilon(z))^{-1/2}$. This results in the peaks broadening and shift towards higher energies.

4. Conclusion and outlook

We have presented the algorithm developed to incorporate the radiative reaction force into the relativistic molecular dynamics framework. The methodology relies on

integrating the equations of motion of an ultra-relativistic particle moving in an external electromagnetic field or passing through a medium. In the latter case, the particle's dynamics is subject to the interaction with all atoms of the medium. The action of the radiative reaction force leads to a gradual decrease in the particle's energy in the course of its motion due to the emission of radiation. The effect of the radiative recoil becomes especially significant for ultra-relativistic projectiles passing through oriented crystals where they are subject to the strong electrostatic crystalline fields. Recent channeling experiments with tens of GeV electrons and positrons [11, 15, 16] have shown the necessity to account for the radiative reaction force in describing the dynamics of the particles.

A case study has been carried out for the initial approbation of the methodology and its implementation in the MBN EXPLORER software package. The simulation of the planar channeling process along with the calculation of spectral distribution of the emitted radiation have been performed for 150 GeV positrons passing through a 200 μm thick single oriented Si(110) crystal. Special attention has been devoted to the trajectory-by-trajectory analysis of the variation of the particle's energy ε with the penetration distance z . Several regimes for the decrease of $\varepsilon(z)$ have been established. One of these corresponds to the channeling motion well away from the atomic planes that are diffused due to thermal vibrations of the atoms. This regime accommodates two thirds of the channeling particles. The radiative energy loss, calculated for the simulated trajectories, is in accordance with the estimate derived using the continuum potential model. The trajectories that have segments close to the diffused atomic planes reveal steeper decrease in $\varepsilon(z)$ due to the events when several sequential distant collisions with the atoms occur along the path. Finally, in a limited number of the trajectories the events of close collisions with the atomic nuclei have been identified. In these collisions the impact parameter (i) is small enough to allow for a noticeable decrease in $\varepsilon(z)$ over the sub-angstrom path, but (ii) large enough for the scattering angle to be much less than the Lindhard critical angle. Hence, after the collision the particle still moves in the channeling mode but with lower total energy.

In the spatial regions where a projectile experiences aforementioned close-encounter collisions the conditions (7) and/or (9) are not met so that the classical description of the radiative energy losses in terms of the radiative reaction force (5) as well as the description of the particle's motion in terms of trajectories become inadequate. In these regions rigorous treatment can only be achieved by means of quantum mechanics. However, taking into account that such events are random, fast and local they can be incorporated into the classical molecular dynamics framework according to their probabilities that are related to the cross sections (i) of the elastic scattering of the projectile from an isolated atom, and (ii) of the bremsstrahlung emission in the static atomic field, see, e.g. [22]. Similar methodology has been already implemented in MBN EXPLORER within the framework of the irradiation-driven molecular dynamics [33].||

|| To be noted that account for random events of inelastic scattering of a projectile from individual atoms that lead to atomic excitation / ionization and to a random change in the direction of the

Algorithmically, to identify these regions, at each step of integration of the equation of motion (1) the validity of inequalities (7) and $\chi < 1$ (see (8)) must be checked. If these conditions are not met then the deterministic classical description is substituted, locally, with the random generation of the kinematic and dynamic quantities in accordance with the known probabilities of the aforementioned processes. We plan to introduce these new features to the numerical algorithm aiming to expand the range of applicability of the code for the trajectories simulations as well as for the calculation of the spectra. Another feature that will be implemented concerns the calculations of the multiphoton emission. This process becomes important for high-energy projectiles channeling in very thick (up to the centimeter range) crystals [16].

Acknowledgments

The work was supported by Deutsche Forschungsgemeinschaft (Project No. 413220201). We acknowledge also support by the European Commission through the N-LIGHT Project within the H2020-MSCA-RISE-2019 call (GA 872196) and the EIC Pathfinder Project TECHNO-CLS (Project No. 101046458). We acknowledge the Frankfurt Center for Scientific Computing (CSC) for providing computer facilities.

Appendix A. Estimation of $\Delta\varepsilon$ for a positron planar channeling

In the channeling regime the velocity of a projectile is oriented (on average) along the plane while the interplanar electric field \mathbf{E} is normal to the plane so that $\langle \mathbf{v} \rangle \perp \mathbf{E}$. Hence, accounting for the conditions

$$\frac{\boldsymbol{\beta} \cdot \mathbf{E}}{E} \ll 1, \quad (\boldsymbol{\beta} \cdot \mathbf{E}) \mathbf{E} \rightarrow 0 \quad (\text{A.1})$$

in (5) one writes the radiative reaction force as follows

$$\mathbf{F}_{\text{rr}} \approx -\frac{2}{3}r_0 \frac{\gamma^2}{mc^2} (eE)^2 \boldsymbol{\beta} \quad (\text{A.2})$$

To estimate the energy loss by an ultra-relativistic projectile due to radiation emission when passing through a crystal of thickness L along $\boldsymbol{\beta}$ ($\beta_z \approx 1$, $\beta_{x,z} \ll 1$) one derives:

$$\frac{\Delta\varepsilon}{\varepsilon} \approx \frac{1}{\varepsilon} \int_0^L |F_{\text{rr},z}| z \approx \frac{2\varepsilon r_0}{3(mc^2)^3} \langle e^2 E^2 \rangle L \quad (\text{A.3})$$

where $\langle e^2 E^2 \rangle$ stands for the average value of the squared force $e\mathbf{E}$ which acts on the channeling particle in a crystal.

Assuming the harmonic approximation for the interplanar potential

$$U(\rho) = \frac{\kappa\rho^2}{2}, \quad \kappa = \frac{8U_0}{d^2}, \quad (\text{A.4})$$

particle's velocity has been already implemented in MBN EXPLORER following the algorithm described some time ago in Ref. [27].

where $\rho = [-d/2, d/2]$ is the distance from the mid-plane, d - interplanar distance, U_0 is the depth of the well. The force acting on the projectile is $eE = \kappa\rho$, therefore, averaging over one period of channeling oscillations with the amplitude a can be carried out analytically:

$$\langle e^2 E^2 \rangle_a = \frac{1}{T} \int_0^T e^2 E^2 dt = \langle e^2 E^2 \rangle_{\max} \left(\frac{2a}{d} \right)^2 \quad (\text{A.5})$$

where

$$\langle e^2 E^2 \rangle_{\max} = \langle e^2 E^2 \rangle_{a=d/2} = \frac{8U_0^2}{d^2} \quad (\text{A.6})$$

Averaging over the amplitudes produces

$$\langle e^2 E^2 \rangle = \frac{2}{d} \int_0^{d/2} \langle e^2 E^2 \rangle_a da = \frac{\kappa^2 d^2}{24} = \frac{\langle e^2 E^2 \rangle_{\max}}{3} \quad (\text{A.7})$$

Table A1. Parameters of the (110) interplanar potentials (at $T = 300$ K) in diamond (C), Si, Ge crystals: d - the interplanar distance, $U_0 = U(d/2)$ - the potential well depth, $\langle e^2 E^2 \rangle$ - see Eq. (A.7), $\langle e^2 E^2 \rangle_{\max}$ - see Eq. (A.6).

	d (Å)	U_0 (eV)	$\langle e^2 E^2 \rangle_{\max}$ (GeV ² /cm ²)
C (110)	1.26	23	26.7
Si(110)	1.92	22	10.5
Ge(110)	2.00	35	24.5

Using the values from Table A1 one derives the following estimates for the relative radiative losses of a positron planar channeling in several oriented crystals:

$$\frac{\Delta\varepsilon}{\varepsilon} = 1.4 \times 10^{-3} \varepsilon \langle e^2 E^2 \rangle L = \varepsilon L \times \begin{cases} 0.012 & \text{diamond(110)} \\ 0.005 & \text{Si(110)} \\ 0.011 & \text{Ge(110)} \end{cases} \quad (\text{A.8})$$

On the right-hand side ε and L are measured in GeV and cm, respectively.

Appendix B. Radiative energy loss in a point Coulomb field: Classical approach

In case when an impact parameter b in a collision of an ultra-relativistic projectile with an atom is much less than the atomic screening radius R one can estimate the radiative energy loss considering the projectile's motion in the Coulomb field of the nucleus. In the small angle scattering limit one assumes the uniform motion along a straight line (the z -axis), $\mathbf{r} \approx \mathbf{b} + z\boldsymbol{\beta}$. Substituting the electrostatic force $\mathbf{F}_{\text{em}} = Ze^2(\mathbf{b} + z\boldsymbol{\beta})/r^3$ into Eq. (5) and carrying out the intermediate algebra one derives the following expression for the relative energy loss $(\Delta\varepsilon/\varepsilon)_s$ in a single close ($b^2 \ll R^2$) collision:

$$\left(\frac{\Delta\varepsilon}{\varepsilon} \Big|_{b < R} \right)_s = \frac{1}{\varepsilon} \left| \int \mathbf{F}_{\text{rr}} \cdot \mathbf{r} \right| \approx \frac{1}{\varepsilon} \left| \int_{-\infty}^{\infty} (\mathbf{F}_{\text{rr}} \cdot \boldsymbol{\beta}) dz \right| \approx \gamma \frac{\pi Z^2}{4} \left(\frac{r_0}{R} \right)^3 \left(\frac{R}{b} \right)^3 \quad (\text{B.1})$$

Here $r_0 = 2.818 \times 10^{-13}$ is the classical electron radius. For the estimation purposes, the Thomas-Fermi radius can be chosen to characterize the screening radius R :

$$R = a_{\text{TF}} = 0.8853Z^{-1/3}a_0 \quad (\text{B.2})$$

where a_0 stands for the Bohr radius. For a silicon atom $a_{\text{TF}} = 0.194 \text{ \AA}$.

Within the same approximation, the scattering angle $\theta_s \ll 1$ as a function of the impact parameter b is given by (see, e.g. [43]):

$$\theta_s \approx \frac{1}{\varepsilon} \left| \int_{-\infty}^{\infty} (\mathbf{F}_{\text{em}} \cdot \boldsymbol{\beta}) z \right| = \frac{2Z r_0 R}{\gamma R b}. \quad (\text{B.3})$$

References

- [1] D. Lietti, E. Bagli, S. Baricordi, A. Berraa, D. Bolognini, P. N. Chirkov, P. Dalpiaz, G. Della Mea, D. De Salvador, S. Hasan, V. Guidi, V. A. Maisheev, A. Mazzolari, M. Prest, E. Vallazza, D. Vincenzi, I. A. Yazynin. Radiation emission phenomena in bent silicon crystals: Theoretical and experimental studies with 120 GeV/c positrons. *Nucl. Instrum Meth. B* **283**, 84 (2012)
- [2] W. Scandale, M. Fiorini, V. Guidi, A. Mazzolari, D. Vincenzi, G. Della Mea, E. Vallazza, A. G. Afonin, Yu. A. Chesnokov, V. A. Maisheev, I. A. Yazynin, A. D. Kovalenko, A. M. Taratin, A. S. Denisov, Yu. A. Gavrikov, Yu. M. Ivanov, L. P. Lapina, V. V. Skorobogatov, D. Bolognini, S. Hasan, M. Prest, Measurement of the dechanneling length for high-energy negative pions. *Phys. Lett.* **B719**, 70 (2013)
- [3] L. Bandiera, E. Bagli, V. Guidi, A. Mazzolari, A. Berra, D. Lietti, M. Prest, E. Vallazza, D. De Salvador, V. Tikhomirov, Broad and Intense Radiation Accompanying Multiple Volume Reflection of Ultrarelativistic Electrons in a Bent Crystal. *Phys. Rev. Lett.* **111**, 255502 (2013)
- [4] E. Bagli, L. Bandiera, V. Guidi, A. Mazzolari, D. De Salvador, G. Maggioni, A. Berra, D. Lietti, M. Prest, E. Vallazza, N. V. Abrosimov, Coherent Effects of High-Energy Particles in a Graded $\text{Si}_{1-x}\text{Ge}_x$ Crystal, *Phys. Rev. Lett.* **110**, 175502 (2013)
- [5] E. Bagli, L. Bandiera, V. Guidi, A. Mazzolari, D. De Salvador, A. Berra, D. Lietti, M. Prest, E. Vallazza, Steering efficiency of a ultrarelativistic proton beam in a thin bent crystal. *Eur. Phys. J. C* **74**, 2740 (2014)
- [6] E. Bagli, L. Bandiera, V. Bellucci, A. Berra, R. Camattari, D. De Salvador, G. Germogli, V. Guidi, L. Lanzoni, D. Lietti, A. Mazzolari, M. Prest, V. V. Tikhomirov, E. Vallazza, Experimental evidence of planar channeling in a periodically bent crystal, *Eur. Phys. J. C* **74**, 3114 (2014)
- [7] U. Wienands, T. W. Markiewicz, J. Nelson, R. J. Noble, J. L. Turner, U. I. Uggerhøj, T. N. Wistisen, E. Bagli, L. Bandiera, G. Germogli, V. Guidi, A. Mazzolari, R. Holtzapple, M. Miller, Observation of Deflection of a Beam of Multi-GeV Electrons by a Thin Crystal, *Phys. Rev. Lett.* **114**, 074801 (2015)
- [8] T. N. Wistisen, U. I. Uggerhøj, U. Wienands, T. W. Markiewicz, R. J. Noble, B. C. Benson, T. Smith, E. Bagli, L. Bandiera, G. Germogli, V. Guidi, A. Mazzolari, R. L. Holtzapple, S. Tucker, Channeling, volume reflection, and volume capture study of electrons in a bent silicon crystal. *Phys. Rev. Accel. Beams* **19**, 071001 (2016)
- [9] E. Bagli, V. Guidi, A. Mazzolari, L. Bandiera, G. Germogli, A. I. Sytov, D. De Salvador, A. Berra, M. Prest, E. Vallazza, Experimental evidence of independence of nuclear de-channeling length on the particle charge sign. *Eur. Phys. J. C* **77**, 71 (2017)
- [10] U. Wienands, S. Gessner, M. J. Hogan, T. W. Markiewicz, T. Smith, J. Sheppard, U. I. Uggerhøj, J. L. Hansen, T. N. Wistisen, E. Bagli, L. Bandiera, G. Germogli, A. Mazzolari, V. Guidi, A. Sytov, R. L. Holtzapple, K. McArdle, S. Tucker, B. Benson, Channeling and radiation experiments at SLAC. *Nucl. Instrum Meth. B* **402**, 11 (2017)
- [11] T.N. Wistisen, A. Di Piazza, H.V. Knudsen, U.I. Uggerhøj, Experimental evidence of quantum radiation reaction in aligned crystals, *Nature Communications* **9** (1), 1 (2018)

- [12] W. Scandale, G. Arduini, F. Cerutti, M. Garattini, S. Gilardoni, A. Masi, D. Mirarchi, S. Montesano, S. Petrucci, S. Redaelli, R. Rossi, D. Breton, L. Burmistrov, S. Dubos, J. Maalmi, A. Natochii, V. Puill, A. Stocchi, D. Sukhonos, E. Bagli, L. Bandiera, V. Guidi, A. Mazzolari, M. Romagnoni, F. Murtas, F. Addesa, G. Cavoto, F. Iacoangeli, F. Galluccio, A. G. Afonin, M. K. Bulgakov, Yu. A. Chesnokov, A. A. Durum, V. A. Maishev, Yu. E. Sandomirskiy, A. A. Yanovich, A. A. Kolomiets, A. D. Kovalenko, A. M. Taratin, G. I. Smirnov, A. S. Denisov, Yu. A. Gavrikov, Yu. M. Ivanov, L. P. Lapina, L. G. Malyarenko, V. V. Skorobogatov, G. Auzinger, T. James, G. Hall, M. Pesaresi, M. Raymond, Comprehensive study of beam focusing by crystal devices *Phys. Rev. Accel. Beams* **21**, 014702 (2018)
- [13] W. Scandale, G. Arduini, F. Cerutti, M. Garattini, S. Gilardoni, A. Lechner, R. Losito, A. Masi, D. Mirarchi, et al., Focusing of 180 GeV/c pions from a point-like source into a parallel beam by a bent silicon crystal. *Nucl. Instrum. Method B* **446**, 15-18 (2019)
- [14] W. Scandale, L. S. Esposito, M. Garattini, R. Rossi, V. Zhovkovska, A. Natochii, F. Addesa, F. Iacoangeli, F. Galluccio, F. Murtas, A. G. Afonin, Yu. A. Chesnokov, A. A. Durum, V. A. Maishev, Yu. E. Sandomirskiy, A. A. Yanovich, G. I. Smirnov, Yu. A. Gavrikov, Yu. M. Ivanov, M. A. Koznov, M. V. Malkov, L. G. Malyarenko, I. G. Mamun, J. Borg, T. James, G. Hall, M. Pesaresi, Reduction of multiple scattering of high-energy positively charged particles during channeling in single crystals *Eur. Phys. J. C* **79**, 99 (2019)
- [15] T. N. Wistisen, A. Di Piazza, C. F. Nielsen, A. H. Sørensen, U. I. Uggerhøj, Quantum radiation reaction in aligned crystals beyond the local constant field approximation. *Phys. Rev. Res.* **1**, 033014 (2019)
- [16] C. F. Nielsen, J. B. Justesen, A. H. Sørensen, U. I. Uggerhøj, R. Holtzappe, Radiation reaction near the classical limit in aligned crystals. *Phys. Rev. D* **102**, 052004 (2020)
- [17] J. Lindhard, Influence of crystal lattice on motion of energetic charged particles. *K. Dan. Vidensk. Selsk. Mat. Fys. Medd.* **34**, 1 (1965).
- [18] E. N. Tsyganov, Some aspects of the mechanism of a charge particle penetration through a monocrystal. Fermilab Preprint TM-682 (Fermilab, Batavia, 1976)
- [19] A. V. Korol, A. V. Solov'yov, W. Greiner. *Channeling and Radiation in Periodically Bent Crystals*, Second ed., Springer-Verlag, Berlin, Heidelberg, 2014.
- [20] M. A. Kumakhov, On the theory of electromagnetic radiation of charged particles in a crystal. *Phys. Lett.* **57A**, 17 (1976)
- [21] E. Uggerhøj, Some recent experimental investigations of photon emission and shower formation in strong crystalline fields. *Rad. Eff. Def. Solids* **25**, 3 (1993)
- [22] V. B. Berestetskii, E. M. Lifshitz, and L. P. Pitaevskii. *Course of Theoretical Physics. Quantum Electrodynamics*, vol. 4. Pergamon Press, Oxford (1982)
- [23] T. N. Wistisen, A. Di Piazza, Complete treatment of single-photon emission in planar channeling. *Phys. Rev. D* **99**, 116010 (2019)
- [24] J. U. Andersen, S. K. Andersen, W. M. Augustyniak, Channeling of electrons and positrons. *K. Dan. Vidensk. Selsk. Mat. Fys. Medd.* **39**, 1 (1977)
- [25] A. Kostyuk, A. V. Korol, A. V. Solov'yov, W. Greiner, Planar channeling of 855 MeV electrons in silicon: Monte Carlo simulations. *J. Phys. B At. Mol. Opt. Phys.* **44**, 075208 (2011)
- [26] A. V. Korol, G. B. Sushko, A. V. Solov'yov, All-atom relativistic molecular dynamics simulations of channeling and radiation processes in oriented crystals. *Eur. Phys. J. D* **75**, 107 (2021)
- [27] A. V. Korol, A. V., Solov'yov, W. Greiner, The influence of the dechanneling process on the photon emission by an ultra-relativistic positron channeling in a periodically bent crystal. *J. Phys. G: Nucl. Part. Phys.* **27**, 95 (2001)
- [28] C. F. Nielsen, GPU accelerated simulation of channeling radiation of relativistic particles. *Comp. Phys. Comm.* **252**, 107128 (2020)
- [29] L. D. Landau, E. M. Lifshitz. *Course of Theoretical Physics, vol. 2 The Classical Theory of Fields*. Pergamon Press, Oxford (1971)
- [30] I. A. Solov'yov, A. V. Yakubovich, P. V. Nikolaev, I. Volkovets, A. V. Solov'yov, MesoBioNano

- Explorer – A universal program for multiscale computer simulations of complex molecular structure and dynamics. *J. Comp. Phys.* **33**, 2412 (2012)
- [31] I. A. Solov'yov, A. V. Korol, A. V. Solov'yov, *Multiscale Modeling of Complex Molecular Structure and Dynamics with MBN Explorer*. (Springer International Publishing, Cham, Switzerland, 2017)
- [32] G. B. Sushko, I. A. Solov'yov, A. V. Verkhovtsev, S. Volkov, A. V. Solov'yov, Studying chemical reactions in biological systems with MBN Explorer: Implementation of molecular mechanics with dynamical topology. *Europ. Phys. J. D* **70**, 12 (2016)
- [33] G. B. Sushko, I. A. Solov'yov, A. V. Solov'yov, Molecular dynamics for irradiation driven chemistry: Application to the FEBID process. *Europ. Phys. J. D* **70**, 217 (2016)
- [34] M. Panshenskov, I. A. Solov'yov, A. V. Solov'yov, Efficient 3D kinetic Monte Carlo method for modeling of molecular structure and dynamics. *J. Comp. Chem.* **35**, 1317 (2014)
- [35] I. A. Solov'yov, G. Sushko, I. Friis, A. V. Solov'yov, Multiscale modeling of stochastic dynamics processes with MBN Explorer, *J. Comp. Chem.* **43**, 1442 (2022)
- [36] G. B. Sushko, I. A. Solov'yov, A. V. Solov'yov, Modeling MesoBioNano systems with MBN Studio made easy. *J. Mol. Graph. Model.* **88**, 247 (2019)
- [37] G. B. Sushko, V. G. Bezchastnov, I. A. Solov'yov, A. V. Korol, W. Greiner, A. V. Solov'yov, Simulation of ultra-relativistic electrons and positrons channeling in crystals with MBN Explorer. *J. Comp. Phys.* **252**, 404 (2013)
- [38] J. D. Jackson. *Classical Electrodynamics* (Wiley, Hoboken, 1999)
- [39] G. Molière. Theorie der Streuung schneller geladener Teilchen I: Einzelstreuung am abgeschirmten Coulomb-Feld. *Z. f. Naturforsch A* **2**, 133-145 (1947).
- [40] L. Fernandes Pacios. Analytical Density-Dependent Representation of Hartree-Fock Atomic Potentials. *J. Comp. Chem.* **14**, 410-421 (1993).
- [41] D. S. Gemmell, Channeling and related effects in the motion of charged particles through crystals. *Rev. Mod. Phys.* **46**, 129-227 (1974)
- [42] V. M. Biryukov, Yu. A. Chesnokov, V. I. Kotov, *Crystal Channeling and its Application at High-Energy Accelerators*. (Springer Science & Business Media, 2013)
- [43] L. D. Landau, E. M. Lifshitz. *Course of Theoretical Physics, vol. 1. Mechanics*. Elsevier, Oxford (2003)
- [44] R. Holtzapple, C. F. Nielsen, A. H. Sørensen, U. I. Uggerhøj & CERN NA63, On the significance of radiation reaction. *Europ. Phys. J. D* **76**, 167 (2022)